SPECTRAL EDDY DIFFUSIVITY AND PRANDTL NUMBER DISTRIBUTIONS IN A HEATED TURBULENT WAKE

Hyung Suk Kang*

Charles Meneveau†
Department of Mechanical Engineering,
and Center for Environmental and Applied Fluid Mechanics,
The Johns Hopkins University,
Baltimore, Maryland 21218, USA

ABSTRACT

For turbulent flows the subgrid-scale (SGS) scalar-variance dissipation spectrum can be expressed as the co-spectrum of negative SGS scalar flux and filtered scalar gradient. Using local isotropy, the radial SGS scalar-variance dissipation spectrum is expressed in terms of the streamwise components of the SGS scalar flux and filtered scalar gradient that can be measured in experiments. Using an array of four X-type hot-wire and four I-type cold-wire probes, two-dimensional box-filtered velocities and temperatures in the streamwise and cross-stream directions by invoking Taylor's hypothesis are obtained at the centerline of a heated wake flow, at a Reynolds number based on Taylor scale of 350. From the radial dissipation spectra the spectral eddy viscosity and Prandtl number are evaluated. Consistent with classical two-point closure predictions, when using box filters, the spectral eddy viscosity and diffusivity decrease near the filter wavenumber. Interestingly, the spectral Prandtl number (the ratio of the spectral eddy viscosity to diffusivity) has a longer plateau-behavior than the spectral eddy diffusivity and viscosity, with a range around 0.7.

INTRODUCTION

In LES, the turbulent fields are decomposed into subgrid scale and resolved scale fields by performing spatial filtering at a scale Δ using a filter kernel, $G_\Delta(\boldsymbol{x})$ (Leonard, 1974; Meneveau and Katz, 2000). The LES equations for the momentum and scalar transport equations include the divergences of the SGS stress tensor τ_{ij} and SGS scalar flux q_j defined as

$$\tau_{ij} \equiv \widetilde{u_i u_j} - \widetilde{u}_i \widetilde{u}_j \tag{1}$$

$$q_j \equiv \widetilde{\theta u_j} - \widetilde{\theta}\widetilde{u}_j \tag{2}$$

where $\widetilde{\ }$ represents a convolution with $G_\Delta(\boldsymbol{x})$, and u_i is the velocity in the i-direction, θ the passive scalar.

To close the momentum and scalar transport equations, the SGS stress tensor and scalar flux must be expressed as functions of the resolved velocity and scalar quantities. Classical isotropic eddy viscosity (ν_T) and diffusivity (γ_T) assume quasi-equilibrium between large and small scales, and read

$$\tau_{ij}^d \equiv \tau_{ij} - \frac{1}{3}\tau_{kk}\delta_{ij} = -2\nu_T \widetilde{S}_{ij} \tag{3}$$

$$q_j = -\gamma_T \widetilde{G}_j \tag{4}$$

where $\widetilde{S}_{ij} \equiv \frac{1}{2}(\partial\widetilde{u}_i/\partial x_j + \partial\widetilde{u}_j/\partial x_i)$ and $\widetilde{G}_j \equiv \partial\widetilde{\theta}/\partial x_j$ are the resolved strain-rate tensor and scalar-gradient vector, respectively. The best-known model for evaluating the eddy viscosity and diffusivity is the Smagorinsky model (Smagorinsky, 1963): both the eddy viscosity and diffusivity are proportional to $\Delta^2|\widetilde{S}|$, where $|\widetilde{S}| = (2\widetilde{S}_{mn}\widetilde{S}_{mn})^{1/2}$. In these formulations, the eddy diffusivities respond equally at all scales of motion, independent of the wavenumber. However, two-point closures such as Direct Interaction Approximation (Kraichnan, 1961) or Eddy Damped Quasinormal Markovian approximation showed that the eddy viscosity (Kraichnan, 1976) and eddy diffusivity (Chollet and Lesieur, 1982) in wavenumber space has to depend upon the wavenumber magnitude.

The radial energy spectrum $E_<(\kappa,t)$ of the filtered velocity and the radial scalar-variance spectrum $E_{\theta<}(\kappa,t)$ of the filtered scalar are defined as follows:

$$E_<(\kappa,t) \equiv |\widehat{G}_\Delta(\kappa)|^2 E(\kappa,t) \tag{5}$$

$$E_{\theta<}(\kappa,t) \equiv |\widehat{G}_\Delta(\kappa)|^2 E_\theta(\kappa,t) \tag{6}$$

respectively, where $\widehat{\cdot}$ is the Fourier mode, and $E(\kappa,t)$ and $E_\theta(\kappa,t)$ are the radial kinetic energy spectrum from the unfiltered velocity and the radial scalar-variance spectrum from the unfiltered scalar field. $E_<(\kappa,t)$ and $E_{\theta<}(\kappa,t)$ (Lesieur, 1990) evolve according to

$$(\frac{\partial}{\partial t} + 2\nu\kappa^2)E_<(\kappa,t) = F(\kappa,t) + T_<(\kappa,t) - H(\kappa,t) \tag{7}$$

$$(\frac{\partial}{\partial t} + 2\gamma\kappa^2)E_{\theta<}(\kappa,t) = T_{\theta<}(\kappa,t) - Q(\kappa,t) \tag{8}$$

where ν and γ are the molecular viscosity and diffusivity, respectively. $F(\kappa,t)$ is the energy injection by large-scale forces, and $T_<(\kappa,t)$ and $T_{\theta<}(\kappa,t)$ are the transfer spectra caused by the resolved scales. The quantities $H(\kappa,t)$ and $Q(\kappa,t)$ are the SGS kinetic energy and scalar-variance dissipation spectra, respectively, and are given by

$$H(\kappa,t) = -\sum_{|\boldsymbol{\kappa}|=\kappa} \widehat{\tau}_{ij}(\boldsymbol{\kappa},t)\widehat{\widetilde{S}}^*_{ij}(\boldsymbol{\kappa},t) \tag{9}$$

$$Q(\kappa,t) = -\sum_{|\boldsymbol{\kappa}|=\kappa} \widehat{q}_j(\boldsymbol{\kappa},t)\widehat{\widetilde{G}}^*_j(\boldsymbol{\kappa},t) \tag{10}$$

where $(\cdot)^*$ is the complex conjugate. The $H(\kappa,t)$ and $Q(\kappa,t)$ represent the kinetic energy and scalar-variance transfer rates

*hskang@jhu.edu
†meneveau@jhu.edu

from a given wavenumber shell $|\boldsymbol{\kappa}| = \kappa$ to the subgrid scales, respectively. In the form of diffusive terms,

$$H(\kappa) = 2\nu_{\rm re}(\kappa, \kappa_\Delta)\kappa^2 E_<(\kappa) \tag{11}$$

$$Q(\kappa) = 2\gamma_{\rm re}(\kappa, \kappa_\Delta)\kappa^2 E_{\theta<}(\kappa) \tag{12}$$

where $\kappa_\Delta = \pi/\Delta$ is the filter wavenumber. These expressions define $\nu_{\rm re}$ and $\gamma_{\rm re}$ as the 'real' spectral eddy viscosity and diffusivity, as measured from the energy and scalar-variance spectra ($E_<(\kappa)$ and $E_{\theta<}(\kappa)$) and the SGS kinetic energy and scalar-variance dissipation spectra ($H(\kappa)$ and $Q(\kappa)$). Also, the 'real' spectral Prandtl number is given by:

$$\Pr(\kappa, \kappa_\Delta) \equiv \frac{\nu_{\rm re}(\kappa, \kappa_\Delta)}{\gamma_{\rm re}(\kappa, \kappa_\Delta)} \tag{13}$$

More details are given in Kang and Meneveau (2005).

The spectral eddy viscosity and diffusivity have been modeled based on the two-point closure, such as EDQNM (Lesieur *et al.* , 1997). In the case of the spectral cutoff filter (Chollet and Lesieur 1981), the modeled spectral eddy viscosity and diffusivity have a plateau behavior for $\kappa/\kappa_\Delta \leq 0.3$, but increase for $0.3 < \kappa/\kappa_\Delta \leq 1$ (cusp behavior) due to the predominantly local energy transfer across the filter scale. The modeled spectral Prandtl number is approximately constant at about 0.6. Langford and Moser (1999) supported the plateau-cusp behavior in the spectral eddy viscosity using DNS.

In the case of the physical (graded) filters, Leslie and Quarini (1979) showed that the EDQNM gives a downward behavior of the eddy viscosity near $\kappa/\kappa_\Delta = 1$ with a non-zero plateau at low wavenumber.

More recently, Cerutti *et al.* (2000) obtained array filtered velocity data at the centerline of a cylinder wake at Reynolds number based on Taylor scale up to 450. When using a spectral cutoff filter in the streamwise direction (with a box filter in the cross-stream direction), a cusp behavior in $\nu_T(\kappa, \kappa_\Delta)$ near the filter scale was observed in agreement with classical two-point closure predictions. For box filters in the both the streamwise and cross-stream directions, a downward behavior in $\nu_T(\kappa, \kappa_\Delta)$ occurred near the filter scale.

Our main objectives in the present study are to derive the SGS scalar-variance dissipation spectrum, to obtain the distributions of $H(\kappa)$, $Q(\kappa)$, $\nu_{\rm re}(\kappa, \kappa_\Delta)$, $\gamma_{\rm re}(\kappa, \kappa_\Delta)$ and $\Pr_{\rm re}$, and to compare the trends with previous results. In order to accomplish these objectives, we directly measure the longitudinal SGS kinetic energy and scalar-variance dissipation spectra sampled at the centerline of a turbulent wake behind a heated cylinder. Then, the longitudinal SGS kinetic energy and scalar-variance dissipation spectra are transformed into each radial SGS dissipation spectrum by using the local isotropy assumption. Finally, the spectral eddy viscosity, eddy diffusivity and Prandtl number are obtained and discussed.

SGS DISSIPATION SPECTRA IN TURBULENCE

For locally isotropic homogeneous turbulence the relation between the radial (H) and longitudinal kinetic energy dissipation spectra ($H_{\tau S}$) was introduced in detail in Cerutti *et al.* (2000) as follows:

$$H(\kappa) = 4H_{\tau S}(\kappa) - \frac{5}{2}\kappa\frac{dH_{\tau S}(\kappa)}{dk} + \frac{1}{2}\kappa^2\frac{d^2H_{\tau S}(\kappa)}{dk^2} \tag{14}$$

where

$$H_{\tau S}(\kappa_1) = -2\langle\widehat{\tau}_{11}(\kappa_1)\widehat{\widetilde{S}}^*_{11}(\kappa_1)\rangle \tag{15}$$

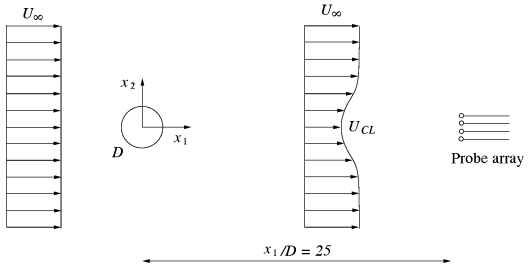

Figure 1: Schematic of cylinder wake flow.

Following a similar derivation in Kang and Meneveau (2005), we can show that the radial SGS scalar-variance dissipation spectrum is determined from its longitudinal dissipation spectrum as follows:

$$Q(\kappa) = 2Q_{qG}(\kappa) - \kappa\frac{dQ_{qG}(\kappa)}{dk} \tag{16}$$

where

$$Q_{qG}(\kappa_1) = -2\langle\widehat{q}_1(\kappa_1)\widehat{\widetilde{G}}^*_1(\kappa_1)\rangle \tag{17}$$

EXPERIMENTAL RESULTS

Experiment apparatus

Experiments are performed in the Corrsin Wind Tunnel (Comte-Bellot and Corrsin, 1966). The length of the test section is 10 m and the size of its cross section is 1.2×0.91 m^2. A schematic of the experimental setup is shown in Fig. 1. A heated smooth cylinder of diameter $D = 4.83$ cm is placed horizontally across the center of the test section. The incoming uniform flow has velocity U_∞. x_1 and x_2 represent the streamwise and cross-stream directions, respectively, and the corresponding velocity components are u_1 and u_2. For the present study, the measurement location is fixed at $x_1/D = 25$ in the streamwise direction at the centerline of the wake flow.

To obtain the filtered quantities, four custom-made miniature probes are used. Each is composed of one X-type hot-wire and one I-type cold-wire for the velocities in the (x_1, x_2)–plane and the temperatures, respectively. The separation distance, h, between the probes in the cross-stream direction (x_2) is 5 mm. We use a filter scale equal to twice the distance between two probes, i.e. $\Delta = 10$ mm.

The signals are sampled at a sampling frequency ($f_s = 40$ kHz) per channel, and low-pass filtered at 20 kHz. The sampling time is 30 seconds, so the total number of data points per channel is 1.2×10^6. Additional details about the experimental setup are provided in Kang and Meneveau (2002).

Characteristics of heated wake flow

Table 1 shows the main parameters of the heated wake flow at the measurement location of $x_1/D = 25$ including the mean centerline velocity U_{CL}, the defect temperature θ_d, the root-mean-square quantities $u_{1\rm rms}$ and $\theta_{\rm rms}$, the molecular kinetic energy dissipation at the centerline ϵ_{CL}, the molecular scalar-variance dissipation at the centerline $\epsilon_{\theta CL}$, the Kolmogorov length scale $\eta = (\nu^3/\epsilon)^{1/4}$, the integral length scale $\ell \equiv 0.9u^3_{1\rm rms}/\epsilon$, and the Taylor micro-scale λ. More detailed information is shown in Kang and Meneveau (2002).

The molecular kinetic energy and scalar-variance dissipation rates ϵ and ϵ_θ are obtained from the third-order structure functions as described in Lindborg (1999) and Kang

Table 1: Parameters of heated wake flow measured at the centerline of the wake at $x_1/D = 25$.

Parameter	$x_1/D = 25$
U_{CL} (ms^{-1})	13.55
U_∞ (ms^{-1})	17.9
$\theta_d = \theta_{CL} - \theta_\infty$ (°C)	0.611
$u_{1\mathrm{rms}}$ (ms^{-1})	1.80
θ_{rms} (°C)	0.251
ϵ_{CL} (m^{2}s^{-3})	87.2
$\epsilon_{\theta CL}$ (°C^{2}s^{-1})	0.648
η (mm)	0.08
$\ell \equiv 0.9u_{1\mathrm{rms}}^3/\epsilon$ (m)	0.060
λ (mm)	2.94
Re_λ	351

and Meneveau(2002). The Reynolds number based on Taylor micro-scale can be calculated from $\mathrm{Re}_\lambda = u_{1\mathrm{rms}}\lambda/\nu$, where $\lambda = \left(15u_{1\mathrm{rms}}^2\nu/\epsilon\right)^{1/2}$, is about 350, as shown in Table 1.

In order to obtain filtered quantities, a two-dimensional box filter is applied to the streamwise and cross-stream directions. The trapezoidal rule is used for the spatial integrations (Cerutti and Meneveau, 2000). In the x_2-direction, a four point discretization is used for evaluating the filtered velocity and SGS stresses. In the streamwise direction, the number of data points inside the box filter is approximated to be $f_s\Delta/\langle u_1\rangle$ and the x_1 derivatives are evaluated using finite differences over a distance h. A three-point approximation is used for the cross-stream derivatives. Filtered gradients in the x_2 direction are evaluated using first-order finite differences over a distance h. More details about the filtering and an error analysis are presented in Cerutti and Meneveau (2000).

Figure 2(a) presents a comparison between the longitudinal spectrum $E_{11}(\kappa_1)$ of the u_1 component and the longitudinal spectrum $E_{22}(\kappa_1)$ of the u_2 component multiplied by 3/4, at the wake centerline. Here, κ_1 is the longitudinal wave number. The vertical dashed line corresponds to the filter scale of $\Delta/\eta = 125$ ($\Delta = 10$ mm). It can be seen that the filter scale is well inside the inertial range. As can be expected from the isotropic turbulence in the inertial range, we observe that $E_{11}(\kappa_1) = \frac{3}{4}E_{22}(\kappa_1)$ over about 1.2 decades of wave number. The detailed discussions and the same spectra in premultiplied form in the study of isotropy are shown in Kang and Meneveau (2001).

Figure 2(b) shows the longitudinal spectrum of the temperature $E_{\theta\theta}(\kappa_1)$. There is a clear inertial range in $E_{\theta\theta}(\kappa_1)$ which coincides with that in $E_{11}(\kappa_1)$ of Fig. 2(a). The cold-wire's frequency response is sufficiently higher than the filter frequency, which indicates that subgrid scales will be well resolved by the cold-wire sensors.

Radial kinetic energy spectrum of the filtered velocity and scalar-variance spectrum of the filtered scalar

The longitudinal energy spectra of unfiltered and two-dimensional box-filtered streamwise velocity, normalized with $\epsilon^{2/3}\Delta^{5/3}$, are shown with non-smooth solid and dashed lines in Fig. 3(a). As in Cerutti *et al.* (2000) and Kang *et al.* (2003), the corresponding three-dimensional radial energy spectrum of the filtered velocity $E_<(\kappa)$ is deduced from the filtered velocity signals by assuming small-scale isotropy.

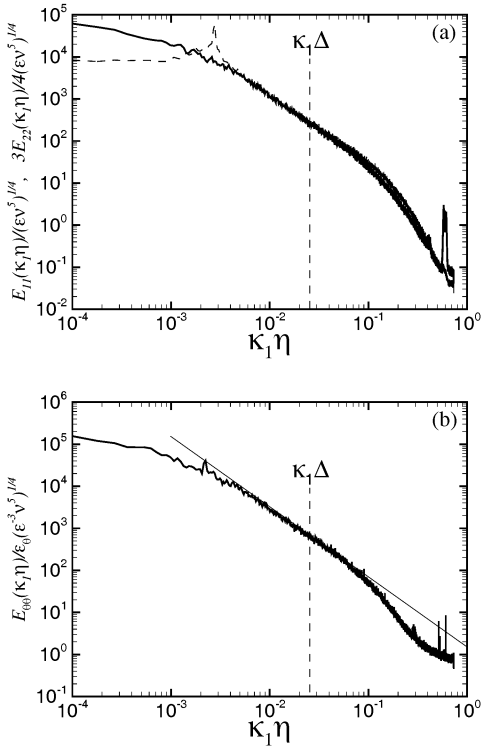

Figure 2: Velocity and temperature spectra in Kolmogorov units (Kang and Meneveau, 2001): (a) the longitudinal spectrum of the u_1 component (solid line) and the longitudinal spectrum of the u_2 component multiplied by 3/4 (dashed line); (b) the longitudinal spectrum of the temperature.

The longitudinal and radial spectra (Pope, 2000) of the filtered velocity are related by

$$E_{11<}(\kappa_1) = \int_1^\infty \frac{x^2-1}{x^3} E_<(\kappa_1 x)\, dx \tag{18}$$

where $x = \kappa/\kappa_1$. The following functional form for the three-dimensional energy spectrum is assumed (Pope, 2000; Cerutti and Meneveau, 2000; Kang *et al.* , 2003):

$$E_<(\kappa) = c_K\epsilon^{2/3}\kappa^{-5/3}\left[\frac{\kappa\ell}{\left[(\kappa\ell)^{\alpha_2}+\alpha_1\right]^{1/\alpha_2}}\right]^{\frac{5}{3}+\alpha_3} e^{-\alpha_4(\kappa\eta)^4} \tag{19}$$

where c_K and α_i ($i = 1$ to 4) are parameters to be decided by comparing with measured $E_{11<}$, and ℓ and ϵ are the integral length scale and dissipation rate as reported in Table 1. The fitted one-dimensional spectrum of the filtered streamwise velocity is visually compared to the measured one, and the procedure is iterated until good agreement between the fitted and measured one-dimensional spectra is achieved. The parameters finally selected are: $c_K = 1.71$, $\alpha_1 = 0.29$, $\alpha_2 = 0.92$, $\alpha_3 = 4.0$, $\alpha_4 = 1.7\times10^{-3}$. The fitted longitudinal spectrum of the filtered streamwise velocity is shown with a smooth solid line in Fig. 3(a), and these values produce good agreement with the measured longitudinal spectrum except the large-scale range ($\kappa_1\Delta < 0.1$). The corresponding three-dimensional radial energy spectrum of $\widetilde{u}_1$ in Eq. (19) is shown with a smooth dashed line in Fig. 3(a).

The longitudinal scalar-variance spectra of unfiltered and two-dimensional box-filtered temperature normalized with

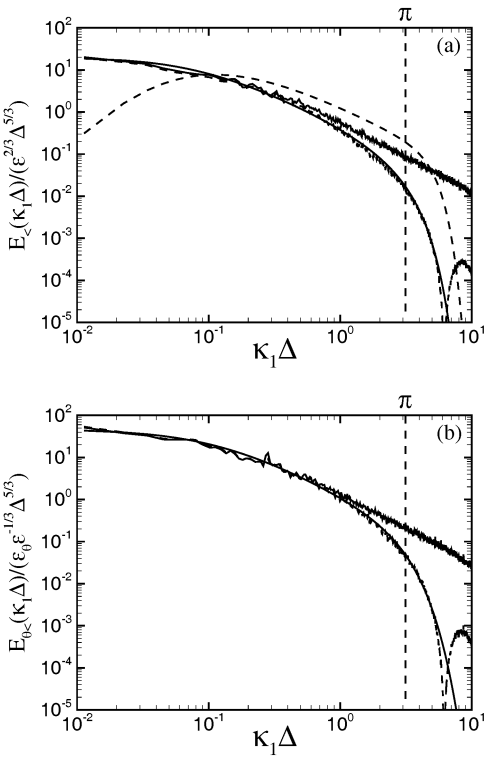

Figure 3: Kinetic energy and scalar-variance spectra. (a) non-smooth solid line: longitudinal energy spectrum; non-smooth dashed line: longitudinal energy spectrum of the two-dimensional box-filtered velocity; smooth solid line: fitted longitudinal energy spectrum; smooth dashed line: radial kinetic energy spectrum of the filtered velocity. (b) non-smooth solid line: longitudinal scalar-variance spectrum; non-smooth dashed line: longitudinal scalar-variance spectrum of the two-dimensional box-filtered temperature; smooth solid line: fitted longitudinal scalar-variance or radial scalar-variance spectrum of the filtered temperature.

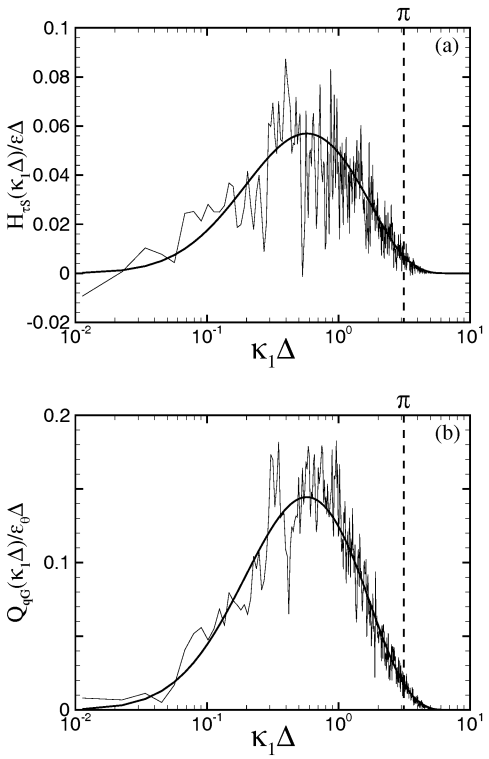

Figure 4: (a) Longitudinal SGS kinetic energy dissipation spectra $H_{\tau S}(\kappa_1)$. (b) Longitudinal SGS scalar-variance dissipation spectra $Q_{qG}(\kappa_1)$. The thin and thick solid lines represent the measured and fitted co-spectra, respectively.

$\epsilon_\theta\epsilon^{-1/3}\Delta^{5/3}$ are shown with non-smooth solid and dashed lines in Fig. 3(b). The radial scalar-variance spectrum of the filtered temperature can be directly obtained from fitting the longitudinal scalar-variance spectrum of the filtered temperature. Similar to the radial kinetic energy spectrum in Eq. (19), the following functional form for the radial scalar-variance spectrum of $\widetilde{\theta}$ is used:

$$E_{\theta<}(\kappa) = c_\theta\epsilon_\theta\epsilon^{-1/3}\kappa^{-5/3}\left[\frac{\kappa\ell}{\left[(\kappa\ell)^{\beta_2}+\beta_1\right]^{1/\beta_2}}\right]^{\frac{5}{3}+\beta_3} e^{-\beta_4(\kappa\eta)^{\beta_5}} \tag{20}$$

where $c_\theta = 1.38$, $\beta_1 = 0.68$, $\beta_2 = 1.2$, $\beta_3 = 0.0$, $\beta_4 = 0.145$. $\beta_5 = 2.0$, and good agreement between the measured and fitted longitudinal scalar-variance spectra of $\widetilde{\theta}$ are obtained as shown with the non-smooth dashed and smooth solid lines, respectively, in Fig. 3(b).

Longitudinal SGS kinetic energy and scalar-variance dissipation spectra

The longitudinal SGS kinetic energy and scalar-variance dissipation spectra, $H_{\tau S}(\kappa_1)$ and $Q_{qG}(\kappa_1)$, are evaluated as the co-spectrum of $-\tau_{11}$ and $\widetilde{S}_{11}$ (Eq. (15)), and of $-q_1$ and $\widetilde{G}_1$ (Eq. (17)), respectively. In terms of data processing, $H_{\tau S}(\kappa_1)$ and $Q_{qG}(\kappa_1)$ are computed from the Fourier transforms of $-\tau_{11}$, $\widetilde{S}_{11}$, $-q_1$ and $\widetilde{G}_1$. The number of segments in the Fourier transform is 576 with overlapping of 50% between the neihgboring segments. The number of samples in each segments is 2^{14}. The measured longitudinal SGS kinetic energy and scalar-variance dissipation spectra are shown with thin solid lines in Figs. 4(a) and 4(b). The dissipation spectra have significant scatter due to lack of complete statistical convergence. However, clear trends of the spectra as functions of $\kappa_1\Delta$ can be observed, including peaks near at $\kappa_1\Delta = 0.6$.

The values of $-\langle\tau_{11}\widetilde{S}_{11}\rangle$ and $-\langle q_1\widetilde{G}_1\rangle$ evaluated in physical space are 8.160 $\mathrm{m^2s^{-3}}$ and 0.171 $(^\circ\mathrm{C})^2\mathrm{s}^{-1}$, respectively. Consistently enough, the values of $\int_0^\infty H_{\tau S}(\kappa_1)d\kappa_1$ and $\int_0^\infty Q_{qG}(\kappa_1)d\kappa_1$ evaluated by integrating the measured longitudinal co-spectra using trapezoidal rule in Fourier space are 8.159 $\mathrm{m^2s^{-3}}$ and 0.170 $(^\circ\mathrm{C})^2\mathrm{s}^{-1}$, respectively. The small under-estimation in Fourier space is likely due to the Hanning windowing applied to the data segment.

Radial SGS kinetic energy and scalar-variance dissipation spectra

The Eqs. (14) and (16) allow us to transform the measured longitudinal SGS dissipation spectra into the radial SGS dissipation spectra. However, the measured longitudinal SGS dissipation spectra are not smooth enough to be differentiated. Therefore, in order to obtain reasonable values of the derivatives in Eqs. (14) and (16), smooth functions are used

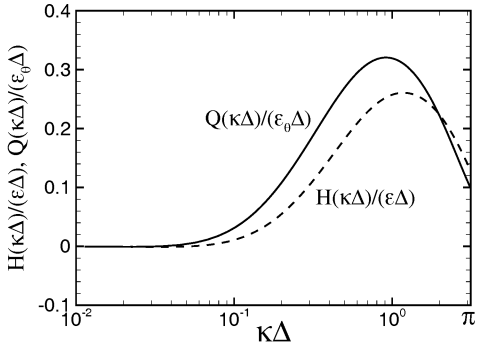

Figure 5: Radial SGS kinetic energy (dashed line) and scalar-variance dissipation spectrum (solid line).

to fit the measured longitudinal SGS dissipation spectra.

A functional form suggested by Cerutti *et al.* (2000) is employed, with a modification to reflect the deviation of the maximum location from the middle point in $\log_{10}(\kappa_1\Delta)$, as follows:

$$\frac{H_{\tau S}^{\rm fit}(\kappa_1)}{\epsilon\Delta} \quad \text{or} \quad \frac{Q_{qG}^{\rm fit}(\kappa_1)}{\epsilon_\theta\Delta} =$$
$$C\exp[c_1(\log_{10}(\kappa_1\Delta)+c_2)^2 + c_3\exp(c_4\log_{10}(\kappa_1\Delta)+c_5)]$$
$$\times[0.5 + c_6\arctan\{c_7(\log_{10}(\kappa_1\Delta)+c_8)\}$$
$$+c_9\exp\{c_{10}(\log_{10}(\kappa_1\Delta)+c_{11})^2\}] \qquad (21)$$

where $c_1 = -1.7$, $c_2 = 0.11$, $c_3 = -0.35$, $c_4 = 3.4$, $c_5 = -0.1$, $c_6 = -0.33$, $c_7 = 20$, $c_8 = -0.71$, $c_9 = 0.14$, $c_{10} = -6$, and $c_{11} = -0.5$. The same functional form is used for both the longitudinal SGS kinetic energy and scalar-variance dissipation spectra except the coefficient C, where $C = 0.067$ for $H_{\tau S}^{\rm fit}(\kappa_1)/(\epsilon\Delta)$ and $C = 0.17$ for $Q_{qG}^{\rm fit}(\kappa_1)/(\epsilon_\theta\Delta)$. The parameters in Eq. (21) are chosen by visual comparison with the measured longitudinal dissipation spectra. The fitted longitudinal SGS kinetic energy and scalar-variance dissipation spectra are shown with thick solid lines in Figs. 4(a) and 4(b), giving good agreements between the measured and fitted spectra except the large scales of $\kappa_1\Delta < 0.2$.

Figures 5 shows the radial SGS kinetic energy and scalar-variance dissipation spectra normalized with $\epsilon\Delta$ and $\epsilon_\theta\Delta$, respectively, obtained from the fitted longitudinal spectra in Eq. (21). Compared to the longitudinal spectra, the peak locations move towards the filter wavenumber, and the peak in the radial kinetic energy dissipation spectrum is closer to the filter wavenumber than that in the radial scalar-variance dissipation spectra.

Spectral eddy diffusivities and Prandtl number

The distributions of the measured real spectral eddy viscosity and diffusivity along the wavenumber are shown in Fig. 6(a). The general trend of $\nu_{\rm re}(\kappa,\kappa_\Delta)$ is similar to the results from Cerutti and Meneveau (2000). At the present Reynolds number, no clear plateau can be observed in either $\nu_{\rm re}(\kappa,\kappa_\Delta)$ and $\gamma_{\rm re}(\kappa,\kappa_\Delta)$. However, broad peaks near $\kappa\Delta = 0.5$ are observed. Consistent with the EDQNM analysis (Leslie and Quarini, 1979), both the measured spectral eddy viscosity and diffusivity with the box filter decrease in the vicinity of the filter wavenumber. The negative values (backscatter) of $\nu_{\rm re}(\kappa,\kappa_\Delta)$ and $\gamma_{\rm re}(\kappa,\kappa_\Delta)$ at the largest

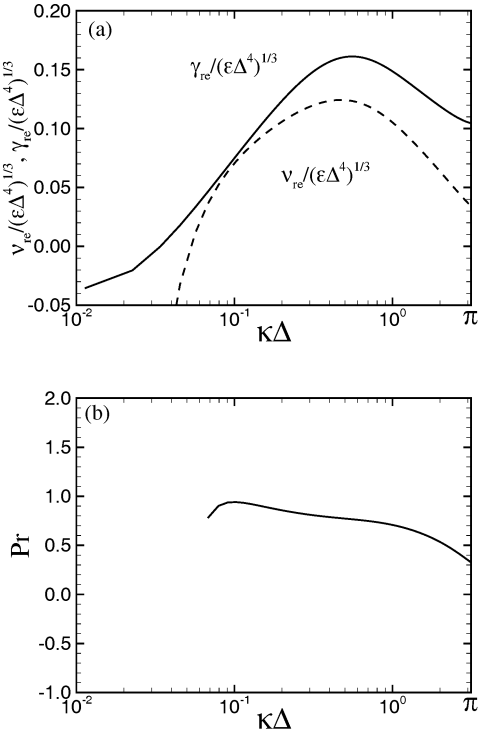

Figure 6: Real spectral properties: (a) Spectral eddy viscosity (dashed line) and eddy-diffusivity (solid line); (b) Spectral Prandtl number.

wavenumbers are associated to the negative, but uncertain, values of $H(\kappa)$ and $Q(\kappa)$. Therefore, the spectral Prandtl number is plotted only for $\kappa\Delta > 0.06$ where eddy diffusivities are positive.

The distribution of the measured spectral Prandtl number $Pr(\kappa,\kappa_\Delta)$ defined as the ratio of $\nu_{\rm re}(\kappa,\kappa_\Delta)$ to $\gamma_{\rm re}(\kappa,\kappa_\Delta)$ is shown in Fig. 6(b). Clearly, the spectral Prandtl number has plateau-downward behavior: a plateau behavior in a range of 0.7–0.9 for $0.2 < \kappa\Delta < 1$. Near the filter wavenumber, the decreasing slope in $\nu_{\rm re}(\kappa,\kappa_\Delta)$ is larger than that in $\gamma_{\rm re}(\kappa,\kappa_\Delta)$, which leads the decrease of the $Pr(\kappa,\kappa_\Delta)$ near the filter wavenumber.

The spectral Prandtl number is lower than 1.0 for $\kappa\Delta < \pi$, however, it is larger than a constant value between 0.3 and 0.6 from the EDQNM predictions (Lesieur *et al.* 1997). This relatively large Prandtl number could be associated with the relatively large c_θ (= 1.38) found in the present flow.

SUMMARY AND CONCLUSIONS

A methodology to measure experimentally the spectral distributions of eddy diffusivity in high-Reynolds-number flows with scalar transport is presented and applied in experiments of high-Reynolds-number shear flow where local isotropy can be assumed. Specifically, the sub-grid scale (SGS) scalar-variance dissipation spectrum is derived as the co-spectrum of negative SGS scalar flux and filtered scalar gradient. Using local isotropy, the result is expressed in terms of the streamwise components of the SGS scalar flux and filtered scalar gradient. Using an array of four X-wire and four cold-wire probes, two-dimensional box-filtered velocities and temperatures in the

streamwise and cross-stream directions by invoking Taylor's hypothesis are obtained at the centerline of a heated wake flow. From the radial SGS kinetic energy and scalar-variance dissipation spectra the spectral eddy viscosity, the spectral eddy diffusivity and the spectral Prandtl number are evaluated. Overall, the measurements yield results in good agreement with important trends predicted by classical two-point closure (Leslie and Quarini, 1979; Lesieur *et al.* , 1997). Specifically, when using box filters, the spectral eddy viscosity and diffusivity decrease near the filter wavenumber. Interestingly, the spectral Prandtl number has a longer plateau-behavior than the spectral eddy diffusivity or viscosity, with a range of 0.7-0.9.

REFERENCES

Cerutti, S., Meneveau, C. and Knio, O. M., 2000, "Spectral and hyper eddy viscosity in high-Reynolds-number turbulence", *J. Fluid Mech.*, Vol. 421, pp. 307-338.

Cerutti, S. and Meneveau, C., 2000, "Statistics of filtered velocity in grid and wake turbulence", *Phys. Fluids*, Vol. 12, pp. 1143-1165.

Chollet, J. P. and Lesieur, M., 1981, "Parameterization of small scales of three-dimensional isotropic turbulence utilizing spectral closures", *J. Atmos. Sci.*, Vol. 38, pp. 2747-2757.

Chollet, J. P. and Lesieur, M., 1982, "Modélisation sous maille des flux de quantité de mouvement et de chaleur en turbulence tridimensionnelle isotrope", *La Météorologie*, Vol. 29-30, pp. 183-191.

Comte-Bellot, G. and Corrsin, S., 1966, "The use of a contraction to improve the isotropy of grid generated turbulence", *J. Fluid Mech.*, Vol. 25, pp. 657-682.

Kang, H. S. and Meneveau, C., 2001, "Passive scalar anisotropy in a heated turbulent wake: new observations and implications for large-eddy simulations", *J. Fluid Mech.*, Vol. 442, pp. 161-170.

Kang, H. S. and Meneveau, C., 2002, "Universality of LES model parameters across a turbulent wake behind a heated cylinder", *J. Turb.*, article 032.

Kang, H. S., Chester, S. and Meneveau, C., 2003, Decaying turbulence in an active-grid-generated flow and comparison with large-eddy simulation", *J. Fluid Mech.*, Vol. 480, pp. 129-160.

Kang, H. S. and Meneveau, C., 2005, "Experimental measurements of spectral eddy diffusivity and Prandtl number distributions in a turbulent wake flow behind a heated cylinder", to be submitted.

Kraichnan, H., 1961, "Dynamics of nonlinear stochastic systems", *J. Mathematical Physics*, Vol. 2, pp. 124.

Kraichnan, H., 1976, "Eddy viscosity in two and three dimensions", *J. Atmos. Sci.*, Vol. 33, pp. 1521-1536.

Langford, J. A. and Moser, R. D., 1999, "Optimal LES formulations for isotropic turbulence", *J. Fluid Mech.*, Vol. 398, pp. 321-346.

Leonard, A., 1974,"Energy cascade in large-eddy simulations of turbulent fluid flows", *Adv. Geophys*, Vol. 18, pp. 237-248.

Lesieur, M., 1990, *Turbulence in Fluids*, Kluwer Academic Publishers.

Lesieur, M., 1997, *Turbulence in Fluids*, Third Revised and Enlarged Edition, Kluwer Academic Publishers

Leslie, D. C. and Quarini, G. L., 1979, "The application of turbulence theory to the formulation of subgrid modelling procedures", *J. Fluid Mech.*, Vol. 91, pp. 65-91.

Lindborg, E., 1999, "Correction to the four-fifths law due to variations of the dissipation", *Phys. Fluids*, Vol. 11, pp. 510-512.

Meneveau, C. and Katz, J., 2000, "Scale-invariance and turbulence models for large-eddy simulation", *Annu. Rev. Fluid Mech.*, Vol. 32, pp. 1-32.

Pope, S. B., 2000, *Turbulent Flows*, Cambridge University Press.

Smagorinsky, J., 1963, "General circulation experiments with the primitive equations. I The basic experiment", *Mon. Weather Rev.*, Vol. 91, pp. 99-116.